HIGH SPEED DIRECT-WRITE FOR RAPID FABRICATION OF THREE-DIMENSIONAL MICROFLUIDIC DEVICES

Ramzi Bey-Oueslati[1], Samy Joseph Palm[2], Daniel Therriault[2], Sylvain Martel[1]

[1]Département de génie informatique, Laboratoire de NanoRobotique
[2]Département de Génie Mécanique, Centre de recherche en plasturgie et composites (CREPEC)
École Polytechnique de Montréal (EPM), 2500 chemin de Polytechnique, Montréal, QC, Canada H3T 1J4
daniel.therriault, sylvain.martel : @polymtl.ca

ABSTRACT

The objective of this research is to adapt the fabrication of cylindrical microchannels by directed assembly for industrial purposes. The directed assembly consists of the extrusion of a fugitive organic ink through a micro-nozzle under constant pressure combined with a layer-by-layer robotic deposition on a substrate for the creation of geometrically complex structures. A multi-axis motion platform has been developed in order to adapt this technique to rapid fabrication. This platform and custom-made software enable the writing of two-dimensional and three-dimensional (2D and 3D) ink networks at a high velocity and positioning accuracy. Improvements on the hardware, software and communication integration were accomplished on this dedicated platform in order to achieve the fast fabrication of precise 3D microstructures. Under similar deposition conditions, the platform developed allowed maximum deposition velocities of more than one order of magnitude superior to the usual writing speeds (i.e., between 1 to 8mm/s). The filaments deposited were characterized by laser scanning profilometry and optical microscopy. The deposition trajectories at high-speed were customized and the smooth roughness of the filament surface was preserved. Finally, the ink structures have been embedded in an epoxy and subsequently removed to create 3D microfluidic networks in order to demonstrate the potential of such platform.

1. INTRODUCTION

Three-dimensional periodic microstructures may find widespread technological applications as sensors [1], composites [2], heat exchangers [3], and in tissue engineering [4]. Current silicon-based technologies require several alignments and bonding processes to create a simple device of a few layers. Eutectic and fusion bonding, for instance, carry the wafer at high temperatures that may not be compatible with the other systems integrated to the device [5]. On the other hand, direct ink and laser writing techniques were used to efficiently produce complex two-dimensional and three-dimensional (2D and 3D) structures with high aspect ratios [6]. Direct ink writing, in particular, is the only microfabrication process capable of creating multilayer periodic structures in a single iteration. However, the integration of microfluidic structures in application devices raises a challenge for the industries. Despite a substantial amount of research invested in microfluidics development, little effort has been devoted to their practical integration. The latter requires attention, and direct ink writing techniques can provide a solution.

The direct-write assembly consists of the robotic deposition of 2D or 3D ink patterns on a substrate [6]-[11]. For the fabrication of microfluidic networks, the process is shown in the Fig. 1. First, an organic ink is extruded through a cylindrical micronozzle under constant pressure. The ink-based pattern is then infiltrated with an epoxy and upon curing, the ink is removed by heating the structure to yield a 2D or 3D microfluidic network comprised of microchannels (~100-250µm in diameter) [12]. In addition, stronger viscoelastic organic inks composed of a microcrystalline wax were designed in order to deposit more complex 3D structures on the substrate [13]. The ink deposition is the critical step of this microfluidic fabrication procedure.

Previous work on direct ink writing of 3D structures includes mesoscale periodic structures fabricated using a robotic deposition rates varying between 2-8mm/s of colloidal inks filaments of cylindrical diameter varying from 100µm to 1mm [8] [9], colloidal ink with a hexagonal shape of vertex-to-vertex diameter of 560µm deposited at 2 mm/s to build 3D structures [10], and smaller 3D scaffolds made of polyamide rich were also produced [11] using a more accurate robot (ABL9000, Aerotech) used for wafers microfabrication prototyping. The diameter of the micro-nozzle was 1µm and the overall dimension of the structures was between 100µm and 200µm. The robotic deposition was performed at 40µm/s. More specific work on microfluidics

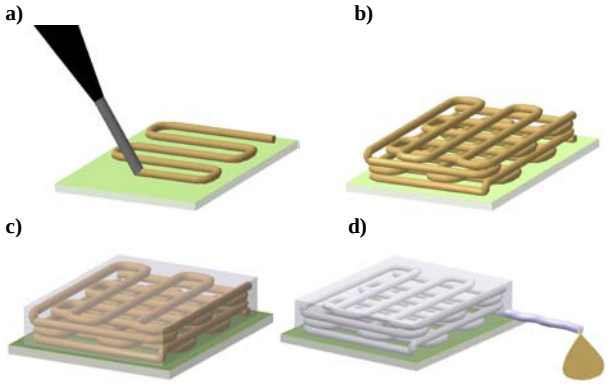

Figure 1: Schematic illustration of the fabrication process for 3D microchannel networks by direct ink writing: a) deposition of the ink through micronozzle; b) layer-by-layer ink deposition; c) epoxy infiltration of network; d) epoxy solidification and removal of fugitive ink.

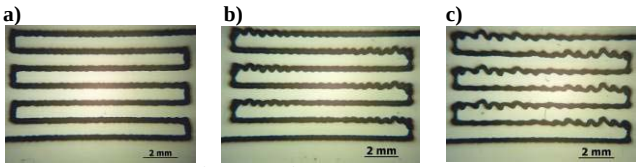

Figure 2: Depositions of 200µm of hydraulic diameter ink patterns using the Fisnar J2200 apparatus. Depositions made at the constant speed of (a) 10mm/s, (b) 20mm/s and (c) 30mm/s.

components has been achieved using an organic ink [13]. Microfluidic devices with hydraulic diameter of 100µm to 250µm have been built [11] [14]. The maximum writing/deposition rates of the channels were between 6mm/s and 8mm/s (JL2000, Robocasting Enterprises, Inc.).

Until now, direct-write techniques are rarely used for industrial mass production mainly because of the slow linear deposition process involved. Although microfluidic devices made using organic ink are of great interest, the writing speeds must be increased in order to demonstrate their viability for high volume production. Commercially available robots such as Cartesian laboratory robots can perform directed assembly technique. Although generally used for non-viscous point-to-point fluid dispensing, thsese robots can also be used for continuous depositions. These robots are economical (~10000-20000$), easy to install and usually come with a user-friendly general-purpose software. A typical example is the J2200 Fisnar or Ultra TT, EFD that enables relatively accurate positioning (repeatability: 10-25µm) at moderate deposition speeds (1-15mm/s), which are appropriate for prototyping purposes. However, these cable drive stages cannot perform tight contour deposition (< 500µm) at high speed (> 15mm/s). Writing rates experiments have been performed using the J2200 which shows to be effective at moderate speeds as shown in Fig. 2. Figures 2b and 2c illustrate that the quality of the microstructures is significantly affected at higher speeds. The increase of the deposition speed to 20mm/s, with a non maximum payload, causes the upper structure to oscillate during direction changes. Moreover, despite the speed limitation, these machines have limited memory for waypoints trajectories and external real-time control is not possible. These limitations must be addressed in order to define the real capabilities of this technique.

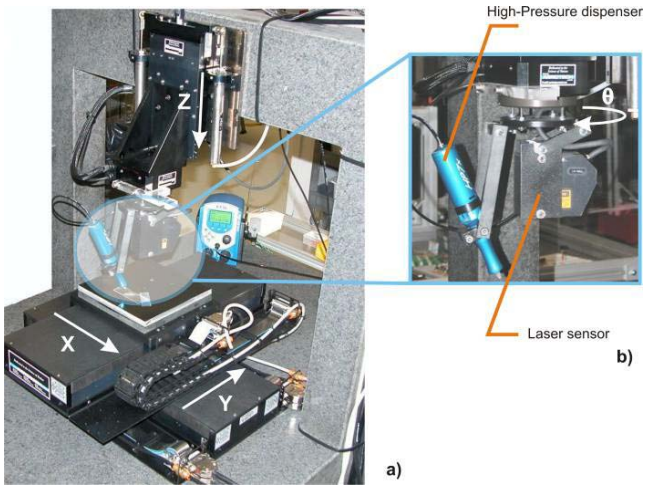

Figure 3: a) Complete experimental setup with four displacement axes placed in gantry configuration, granite structure, air dispenser, mechanical valve and the syringe. The two horizontal displacement robots (ALS25000, Aerotech) place in Cartesian configuration. b) The rotary stage (ADRS150, Aerotech) mounted under the vertical stage (AlS130, Aerotech) in a cylindrical configuration.

Here, we present significant advancements for high speed and accurate ink deposition for the creation of 3D microfluidic devices. A new high performance robotic platform with custom coded software was assembled successfully. The high-speed depositions achieved with this platform under different speeds, geometries, ink-viscosities and diameters were characterized by laser scanning profilometry and optical microscopy.

2. EXPERIMENTAL SETUP

The platform designed for high-speed microfabrication by direct-write assembly consists of a four degree of freedom positioning stage that accurately moves the extrusion system and/or the substrate at speeds reaching 88mm/s for continuous three-dimensional motions and up to 100mm/s for two-dimensional patterns. For maximum stage velocity and accuracy, a combination of Cartesian, cylindrical and gantry configurations was selected for the design of the deposition platform, as shown in Fig. 3a. Linear servo motors with linear mechanical bearings were used for the XY and Z positioning. The axes are separated into two groups of two (i.e., axes x and y; axes z and θ) in order to minimize the system inertia. The two positioning groups are fixed onto a massive custom-made granite structure (~ 1000 kg, Standridge Granite Corp.) for high dynamic stability of the platform during operation. The flatness of the granite structure was controlled (~ 2µm/ft) in order to maintain proper alignment between the two positioning groups over the whole traveling range. A high capacity air-piston table (pressure of 652 kPa, 68-500 Series, Harvard Apparatus Canada) ensures the active damping of oscillations caused by the stage motions during depositions.

The displacement bearings for horizontal motion of Fig. 3a are supported by large cross-sections while still maintaining an overall low profile to decrease deviations in straightness and flatness. The short distance between the bearings combined with a linear DC amplifier enable superior contour-motion profiles. This design has been selected in order to deposit dense parallel microchannels at high speed. A center-driven linear motor, which is controlled by a pulse width modulation (PWM) digital amplifier, is used for vertical positioning. Two pneumatic counter-balances have been adjusted on both sides of the stage to simulate a zero gravity environment when the motor is not powered. The fourth degree of freedom is provided by a rotary direct-drive brushless servomotor mounted under the vertical axis, which is also controlled by a PWM digital amplifier. The four amplifiers are interconnected, and controlled through a firewire (IEEE-1394) connection to a computer.

A high-pressure dispenser (HP7x, EFD) is mounted on a metallic holder under the rotary motor. This dispensing tool contains a 3cc syringe barrel and a piston that multiplies the input air pressure by a factor of 7. An air-operated dispenser (Ultra 2400, EFD) is used to regulate the air pressure from 0 to 689 kPa via the parallel port of the computer. As shown in Fig. 3b, a laser scanner (LK-G82, Keyence) has been mounted next to the syringe for roughness measurements.

This laser system uses a CCD lens to measure the distance by triangulation with a resolution of 0.2µm.

3. SOFTWARE ENVIRONMENT

The deployment of any industrial microfabrication platform involves a substantial amount of software development. How the positioning system is programmed, configured and controlled has an important influence on its performance. At the microscale, geometries imposed by the structures may involve millions of waypoints in order to keep a desired level of precision, and to conserve a constant velocity vector among all axes. To obtain conformed structures, the waypoints need to be synchronized on all positioning axes. Therefore, the need for a hard real-time system (i.e., response time in the order of ~µs) is necessary.

3.1 System architecture

A C/C++ class library combined with a Win32 application programming interface (API) has been developed in order to provide real-time intuitive control of the platform. This interface is running over Windows XP on a standard PC (Intel Pentium 4, 3.2 GHz, 512 MB of RAM). As opposed to programmable logic controllers (PLC), computer-based automations involve real-time responses at the PC level and interruptions in Windows XP/2000 cannot be managed in less than 100 ms. While Windows Embedded products can provide a hard real-time environment on a PC, the drivers' interface hardware needs to be programmed when not provided by manufacturers. Real-time Linux also offers very serviceable performance for real-time processing, yet most component-manufacturers do not provide Linux drivers. As a result, the Real-Time Extension (RTX) runtime environment proved to be the best choice for this platform operating under Windows. Its kernel runs besides Windows kernel to provide precise control of interrupt requests, input/output accesses and memory without interfering with Windows' infrastructure as presented in Fig. 4a. It provides deterministic time-responses to real-time applications, and its typical thread latency service interruptions are less than 1µs.

Fig. 4b presents the architecture of the motion system used. A part of the RAM is reserved during the initialization

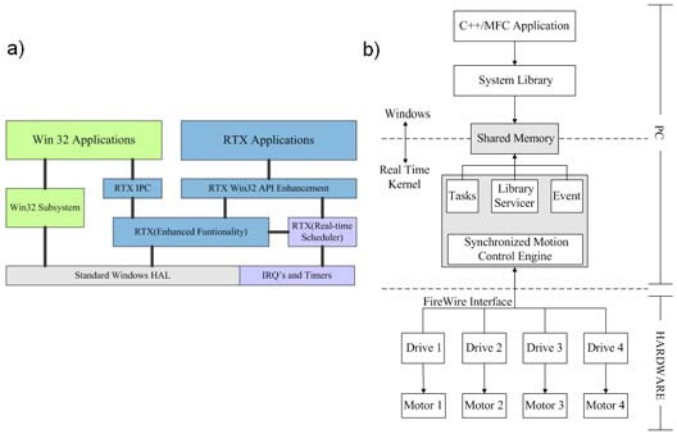

Figure 4: a) RTX software diagram. The hardware abstraction layer (HAL) of RTX provides resources for a real-time clock (shortest period of 100 µs) and an insulation of the interruptions set by RTX over layers. The Real-Time SubSystem (RTSS), which provides the functions and resources management, is simply a hardware driver installed on Windows. b) Positioning system hardware/software simplified diagram.

for the direct communication with the firewire interface. This procedure avoids the pagination and swapping of that memory that slows down the communication by a factor of approximately one million due to hard drive access. Commands sent by the application through the system library are processed on a first priority fixed by RTX, and queued in that shared memory. The synchronized motion control engine manages the subsequent communication protocols, thus ensuring that the right command is sent to the right microcontroller. The same communication channel is used for the information transmitted from the controllers to the applications. This configuration allows millions of points physically separated by a few tens of microns to be sent on a limited sized memory, and processed by the stage microcontrollers with acceptable latency delays.

3.2 Curve parameterization

Deposition trajectories such as sharp corners are difficult to deposit at high-speed because of the abrupt changes in direction. The displacement system incorporates a continuous motion option, which allows the platform to keep an apparent constant speed during the whole deposition process. As such, the controller executes a subtle round corner, and increases the current to the motors, thus maximizing the acceleration in the new direction vector. If it exceeds the available or possible current, a flag is asserted and the stage is stopped. Since the filament is deposited at a constant pressure for a given speed, any mismatch between the extrusion linear flow rate and the stage velocity will alter the diameter of the ink filament. This parameter is even more important for multi-layer structures since the integrity of each layer depends on the supporting layers underneath. Thus, we applied and tested a B-Spline algorithm on control points sent by the user in order to reach a maximum and stable velocity for different deposition trajectories. The B-Spline curve is defined over a parameter u, using the following equation [15]:

$$C(u) = \sum_{i=0}^{n} P_i N_{i,p}(u) \tag{1}$$

$$N_{i,0}(u) = \begin{cases} 1 \Rightarrow u_i \le u \le u_{i+1} \\ 0 \Rightarrow otherwise \end{cases} \tag{2}$$

$$N_{i,p}(u) = \frac{u - u_i}{u_{i+p} - u_i} N_{i,p-1}(u) + \frac{u_{i+p+1} - u}{u_{i+p+1} - u_{i+1}} N_{i+1,p-1}(u) \tag{3}$$

where $C(u)$ represents the new curve varying between u_{min} and u_{max} defined as the nodal vector, the n+1 control points are denoted P_i, the basic functions are denoted $N_{i,p}$ and p is the degree of the curve. B-Spline curves are defined inside the convex envelopes of the control points, which prevent any unwanted contact between the channels. As shown in Eq. 2, the basic functions are defined only on a limited band depending on the corresponding value on the nodal vector. Higher degree curves are calculated, as shown in Eq. 3, by a recursive algorithm. This local support offered by the B-Spline makes it prompt and easy to use with a standard computer. A third degree parameterized curve of 100,000 three-dimensional points may be computed in 5 minutes.

The applied algorithm does not necessarily degenerate the shape of the desired structure as in Fig. 5a. On the other

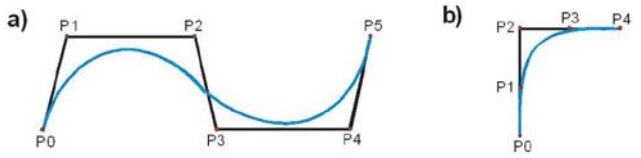

Figure 5: a) B-Spline curve. b) Isolation of a corner using the B-Spline algorithm.

hand, this structure can be sampled before applying the algorithm, thus isolating the sharp corners as shown on Fig. 5b. The curvatures of the microchannels could also be defined using the B-Spline algorithm. At a given point, the curvature is calculated using Eq. 4 for a parametric curve in a Cartesian plan (x, y):

$$R = \frac{(x'^2 + y'^2)^{\frac{3}{2}}}{(x'y'' - y'x'')}. \quad (4)$$

4. RESULTS AND DISCUSSION

4.1 Ink characterization

The organic ink used for the deposition is a binary mixture of microcrystalline wax and a lower molecular weight organic phase (gel petroleum). The ink's elasticity increases linearly with increasing weight fraction of the microcrystalline wax [12]. The ink design is function of three major constraints. First, the cylindrical shape of the extruded ink filament must remain unchanged after the extrusion. Second, the ink mixture must be strong enough to self-support several superimposed layers. Finally, the viscosity of the ink must allow the extrusion through a micronozzle within the maximum applicable pressure available in the experimental setup (4826 kPa in our particular case). Previous work [13] shows that 10 to 40 of weight percent (wt-%) microcrystalline wax exhibits excellent printing behavior under ambient conditions. Using a modest applied pressure, the optimal ink composition is 40wt-%. As shown in Fig. 6, the required pressure for an extrusion that would maintain the proper filament diameter (i.e. 200µm) during 2D deposition increases linearly with the deposition speed for an ink with 20wt-%, 30wt-% and 40wt-% microcrystalline waxes. Therefore, the usage of an ink composition of 40wt-% would be limited to a speed of

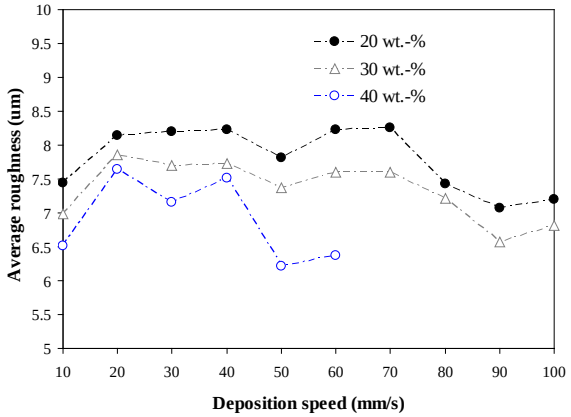

Figure 7: Average roughness of deposited filaments made of binary ink mixtures (20wt-% and 40wt-% microcrystalline waxes) for various speeds.

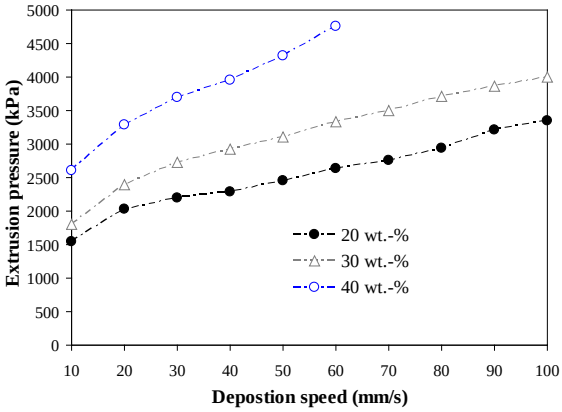

Figure 6: Extrusion pressure required to maintain a 200µm ink diameter during the deposition for inks containing 20% and 40% of microcrystalline wax.

60mm/s for a nozzle with an inner diameter of 200µm because the required extrusion pressure would reach the maximum capacity of the setup. The less viscous inks allow higher deposition speeds without compromising the integrity of the extruded filament. The applied pressure for the ink at 20wt-% and 30wt-% of wax during 2D depositions at speeds varying from 10 to 100mm/s are presented in Fig. 6. At 100mm/s, the pressure required for the deposition of the organic ink is 4006 kPa and 3354 kPa respectively, which is still below the maximum pressure of 4826 kPa of the dispenser.

The 20wt-% and 30wt-% ink allows a higher deposition velocity while presenting lower shape retention of the filaments compared to the 40wt-% ink. The polymer channel walls were previously measured [12] with a root-mean-square surface roughness of 13.3±6.5nm using a stylus instrument with high sampling rates. Here, the average roughness of the ink was measured with lower sampling on longer distances in order to determine the deviation of nominal diameter for the different mixtures at different applied pressures and deposition speeds. The average roughness of the ink filament was measured using the laser system presented in Section 2. The measurements were done on the mid section of straight 200µm filaments for the three different mixtures (20wt-%, 30wt-%, 40wt-%) at different velocities and are presented in Fig. 7. The average roughness (R_a) is calculated using (ASME B.46.1):

$$R_a = \frac{1}{L}\int_{x=0}^{x=L} |y|\, dx \quad (7)$$

where L is the length of the measured profile, and y is the distance from the centre line. Surfaces with known roughness have been tested to validate our roughness measurements, and thus, the laser's light intensity was adjusted to properly reflect on the ink which is a half transparent material. The distance measurements were done every 1.1µm over a length of 8 mm. The extrusion pressure was set according to the values presented in Fig. 6. A small increase of 1 to 3µm of the filament roughness has been observed when using the 20wt-% and 30wt-% mixture compared to the 40wt-% for writing speeds between 10 to 60mm/s as shown in Fig. 7. The 40wt-% ink presents an average R_a of 6.9µm through the different speeds and pressures with a standard deviation of 0.62µm. This average is 7.8µm for the 20wt-% ink with a standard deviation of 0.47µm and 7.3µm for the 30wt-% ink

with a standard deviation of 0.43µm. Although further investigations are required, the ink's slight differences in roughness under different writing speeds may be due to the rheological response of the ink under different pressures. However, the roughness or the shapes of straight-deposited filaments do not restrain the writing speeds.

4.2 Parameterized depositions

The B-Spline algorithm has been tested for the writing of a 90 degree path at 40mm/s using a filament with a diameter of 100µm. As shown in Fig. 8a, the channel does not preserve its shape during the sharp turn. The sudden change of direction and the resulting acceleration are damageable for the quality of the channels. Figure 8b presents a filament written under the same conditions but using a B-Spline parameterization. This third degree curve is defined with a 200µm step and was calculated in less than a second. The resulting deposited filament is smooth, has a regular cross section and adheres well on the substrate surface.

The deposition was performed under a constant applied pressure for a given nozzle diameter and a deposition speed as in Fig. 6 for a 200µm nozzle. Due to the mechanical time response of the dispensing system used, the applied pressure cannot be rapidly changed in order to maintain a constant filament diameter. Therefore, the goal is to minimize the velocity deviation from the desired value during the writing process even for intense curvature paths. Figure 9a shows the velocity error along the X and Y displacement axes for a 90-degree turn trajectory as shown in Fig. 8a. The absolute maximum velocity error is 72µm/s for the X axis and 40µm/s for the Y axis. Figure 9b shows the errors when using the parameterization algorithm and reductions to 51µm/s for the X axis and 31µm/s for the Y axis are observed. It has also been observed that the transition of the motion from the Y axis to the X axis is much more gradual since it involves a higher quantity of control points. The error for the X axis is slightly higher because of the higher inertia due to the mass of the Y axis motor.

4.3 Three-dimensional depositions

A high aspect ratio 3D scaffold, presented in Fig. 10, has been fabricated at 88mm/s using the 20wt-% microcrystalline wax mixture. This 3D scaffold consists of a 54-layer structure of parallel cylindrical rods of 200µm (d) with an inter-rod separation distance (L) of 1.25 mm (L/d=6.25). The resulting 3D network is a 20 mm × 20 mm × 9.18 mm structure made of a 19.6m ink filament. The proper alignment of the 54 layers is shown in Fig. 10b. A similar structure of 104 layers was previously produced [13] at a

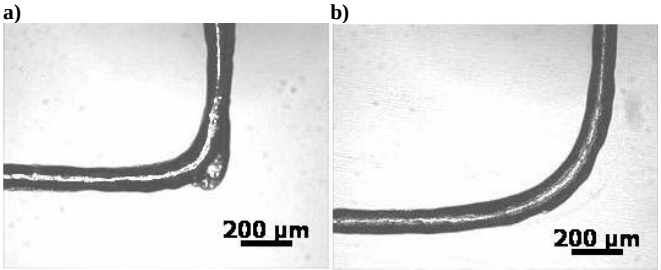

Figure 8: a) 90-degree corner written with a 100µm filament. **b)** Smoothened corner using B-Spline algorithm written with a 100µm filament.

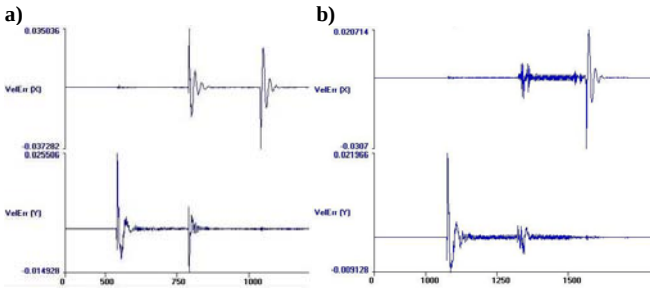

Figure 9: X and Y (horizontal displacements stage) velocity error inmm/s versus time in ms during the deposition of a **a)** 90-degree turn written with a 100µm filament. **b)** Smoothened 90-degree turn using a B-Spline algorithm written with a 100µm filament.

speed of 8mm/s. Even if the writing speed is superior by a factor of more than 10, the 20wt-% microcrystalline wax mixture was not able to support 104 layers. After 54 layers, the structure slowly started to collapse under its own weight. Thus, the preprogrammed routine failed because the superimposed layers have to be written at a specific vertical offset distance of 170µm. Also, the binary mixture made of 30wt-% of microcrystalline wax seems to be more appropriate for a high number of superimposed layers. According to the linear relationship between the extrusion pressure and the deposition speed, this mixture would allow high velocity writing with a higher stiffness. However, the less viscous mixture made of 20wt-% shows a better behavior on continuous dispensing of 3D structures at high velocity.

The 3D scaffold structure has been embedded in an epoxy and cleaned using hot water and high air pressure. Figure 10c shows the resulting microchannel network filled with a fluorescent fluid. The fugitive ink filament (diameter of 200µm) made of 20wt-% microcrystalline wax shows no deformation on a spanning distance of 1.25mm and was not damaged during the epoxy infiltration.

4.4 Microfluidic devices

2D and 3D microfluidic networks can easily be produced with this microfabrication technique. As depicted in Fig. 11, the inks filament can intersect for more sophisticated fluidic designs. Figure 12 shows an example of a microvascular network made of two superimposed and intersecting layers of microchannels (250µm in diameter) deposited with the high performance platform at the speed of 88mm/s. The geometry of the structure is made of parallel diagonal filaments for which the two axis (X and Y) needs to move simultaneously. The writing of the ink filament has been done over a polymethyl polymethacrylate (PMMA) substrate. An epoxy is used as adhesive on multilayer PMMA microfluidic components [16]. The adhesion has bond strengths that prevented delamination or leakage during the ink removal

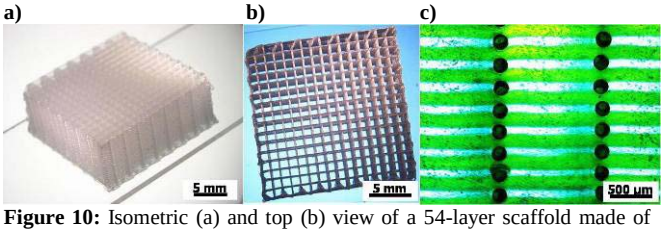

Figure 10: Isometric (a) and top (b) view of a 54-layer scaffold made of binary organic ink (20 wt-% microcrystalline wax) deposited through a 200 µm nozzle at a speed of 88 mm/s. c) Scaffold filled with a fluorescent fluid after an epoxy infiltration and the removing of the fugitive ink.

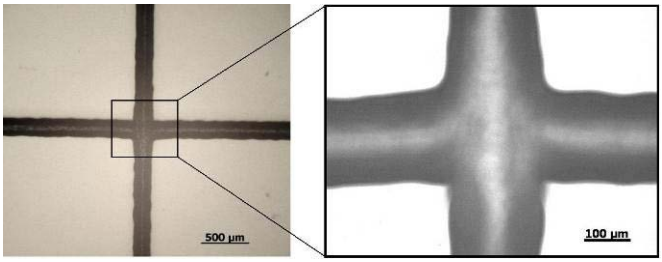

Figure 11: Intersection of filaments of 200µm of diameter made at constant vertical position with a 20wt-% mixture ink.

process which involves a temperature of 60°C and an air pressure of 620kPa applied inside the microchannels network. The three-dimensional microfluidic component is 2.6mm thick where the epoxy only holds 1mm of thickness. An inlet and an outlet have been incorporated in the component for the cleaning and filling of the network. These inlets/outlets are ink filaments deposited and located outside of the main structure. Finally, micro-tubes (S-54-HL, Tygon) were aligned and fixed to the device in order to allow the filling of the network using a needle of 230µm of outer diameter.

5. CONCLUSION

We have adapted the direct ink writing technique for the high-speed fabrication of 2D and 3D microfluidic devices. The fabrication time is critical for high volume production in the industry. The robotic platform and custom-made software presented in this paper have significantly enhanced the deposition performance. Previously performed between 2mm/s to 8mm/s, 2D depositions can now be achieved at a maximum velocity of 100mm/s and high aspect ratio 3D periodic microstructures were fabricated up to 88mm/s while preserving structural integrity. Viscoelastic properties of the 20wt-% microcrystalline wax ink mixture are the most suitable for high velocity depositions due to lower micro-extrusion pressure. This less viscous mixture allowed increasing the deposition speed but restricted the possible amount of superimposed layers (50%) and it also slightly increased the average roughness of the channels (~1-2µm) compared to the optimal ink composition (40wt-%). However, this ink was successfully used for the writing of 200µm of hydraulic diameter channels to build 3D microfluidic devices. Several other deposition parameters such as ink elasticity, nozzle inner diameter and structure geometry have an important impact on the final microfluidic component quality and should be fully characterized. Parallel writing is also investigated for a complete optimization of the deposition process Advances in computer engineering and automation science will eventually enable the integration of direct writing microfabrication to the industry for the mass production of 3D microfluidic devices.

6. ACKNOWLEDGMENT

This work is supported by a strategic grant from the Natural Sciences and Engineering Research Council of Canada (NSERC) and in part by a Canada Research Chair (CRC) in Micro/Nanosystem Development, Fabrication, and Validation, the Canadian Foundation for Innovations (CFI) and the Government of Québec. The authors acknowledge the help of Jean-Baptiste Mathieu and Martin Mankiewicz as well as the team members of the Micro Heat Pipe project.

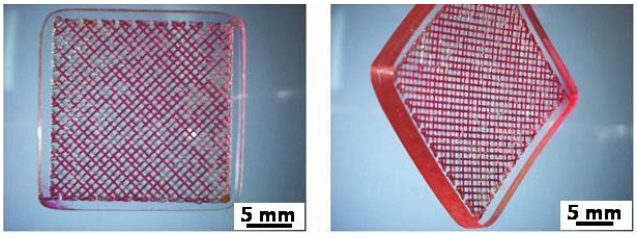

Figure 12: Top (a) and isometric (b) views of a 2 layer microchannel network (250µm of diameter) filled with a colored fluid.

7. REFERENCES

1. H. Yu, O. Balogun, B. Li, et al. Fabrication of Three-Dimensional Microstructures Based on Singled-Layers SU-8 for Lab-on-Chip Applications. *Sensors and Actuators A-Physical.* vol. 127, no. 2, pp. 228-234, 2006.

2. G. T. Vladisavljevic and R. A. Williams, Recent Developments in Manufacturing Emulsions and Particulate Products Using Membranes. *Advances in Colloid and Interface Science*, vol. 113, no. 1, pp. 1-20, 2005.

3. M. Lee, M. Wong and Y. Zohar, Integrated Micro-Heat-Pipe Fabrication Technology. *Journal of Microelectromechanical Systems.* vol. 12. pp. 138-146, 2003.

4. J. J. Norman and T. A. Desai, Control of Cellular Organization in Three Dimensions Using a Microfabricated Polydimenthylsiloxane. *Tissue Engineering*,vol. 11, no. 3-4, pp. 378-386, 2005.

5. M. Madou, *Fundamentals of Microfabrication*,CRC Press, Boca Raton, Flo., chap. 8, 1997.

6. J. A. Lewis and G. M. Gratson, Direct Writing in Three Dimensions. *Materials Today*, 7, 289-293, 2004.

7. G. M. Gratson, M. J. Xu, J. A. Lewis, Microperiodic structures - Direct writing of three-dimensional webs, *Nature*, vol. 428, pp. 386-386, 2004.

8. J. E. Smay, J. Cesarano and J. A. Lewis, Colloidal inks for directed assembly of 3-D periodic structures. *Langmuir*, vol. 18, pp. 5429-2437, 2002.

9. J. E. Smay, G. M. Gratson, R. F. Shepherd, J. Cesarano and J. A. Lewis, Directed Colloidal Assembly of 3D Periodic Structures. *Advanced Materials*, 14, pp. 1279, 2002.

10. R. B. Rao, K. L. Krafcik, A. M. Morales and J. A. Lewis, Microfabricated Deposition Nozzles for Direct-Write Assembly of Three-Dimensional Periodic Structures. *Advanced Materials*, vol. 17, pp. 289-293, 2005.

11. M. J. Xu, G. M. Gratson, E. B. Duoss, R. F. Shepherd and J. A. Lewis, Biomimetic Silicification of 3D polyamine-rich scaffolds assembled by direct ink writing, *Soft. Matter.*, vol. 2, pp. 205-209, 2006.

12. D. Therriault, S. R. White, and J. A. Lewis, Chaotic Mixing in Three-Dimensional Microvascular Networks Fabricated by Direct-Write Assembly. *Nature Materials*, vol. 2, pp. 265-271, 2003.

13. D. Therriault, R. Shepherd, S. R. White, and J. A. Lewis, Fugitive inks for direct-write assembly of three-dimensional microvascular networks. *Advanced Materials*, vol. 17, pp. 395-399, 2005.

14. J. B. Mathieu and S. Martel, Magnetic steering of iron oxide microparticles using propulsion gradient coils in MRI, *Proc. Annual International Conference of the IEEE Engineering in Medicine and Biology Society*, 2006.

15. W. M. Newman and R. F. Sproul, *Principles of Interactive Computer Graphics*. 2nd ed. New York: McGraw-Hill, pp. 309-331, 1979.

16. B. R. Flashbart, K. Wong, J. M. Iannacone, E. N. Abante et al., Design and fabrication of a multilayered polymer microfluidic chip with nanofluidic interconnects via adhesive contact printing, *Lab Chip*, vol. 6, pp. 667-674, 2006.